Nanoscale

RSC Publishing

PAPER

View Article Online
View Journal | View Issue

Published on 12 April 2013. Downloaded by UNIVERSITY OF NEBRASKA on 16/07/2013 09:18:29.

Cite this: *Nanoscale*, 2013, **5**, 5426

Highly selective gas sensor arrays based on thermally reduced graphene oxide

Alexey Lipatov,[a] Alexey Varezhnikov,[b] Peter Wilson,[a] Victor Sysoev,[b] Andrei Kolmakov*[c] and Alexander Sinitskii*[ad]

Received 11th February 2013
Accepted 10th April 2013

DOI: 10.1039/c3nr00747b

www.rsc.org/nanoscale

The electrical properties of reduced graphene oxide (rGO) have been previously shown to be very sensitive to surface adsorbates, thus making rGO a very promising platform for highly sensitive gas sensors. However, poor selectivity of rGO-based gas sensors remains a major problem for their practical use. In this paper, we address the selectivity problem by employing an array of rGO-based integrated sensors instead of focusing on the performance of a single sensing element. Each rGO-based device in such an array has a unique sensor response due to the irregular structure of rGO films at different levels of organization, ranging from nanoscale to macroscale. The resulting rGO-based gas sensing system could reliably recognize analytes of nearly the same chemical nature. In our experiments rGO-based sensor arrays demonstrated a high selectivity that was sufficient to discriminate between different alcohols, such as methanol, ethanol and isopropanol, at a 100% success rate. We also discuss a possible sensing mechanism that provides the basis for analyte differentiation.

Chemical sensing is one of the most attractive applications of graphene, considering the exceptional sensitivity of graphene-based electronic devices to the surface adsorbates.[1] Another interesting material for gas sensing applications is graphene oxide (GO), a two-dimensional (2D) carbon-based material with different oxygen-containing functionalities, which is produced by an oxidative exfoliation of graphite.[2,3] Heavily oxidized GO is not electrically conductive.[4,5] However, GO could be transformed to a conductive material *via* reduction when most of the oxygen-containing functionalities are removed using either a reducing agent, such as hydrazine, or high-temperature annealing.[2,3] The resulting reduced graphene oxide (rGO) has inferior electrical properties compared to pristine graphene,[4–6] but it is sufficiently conductive to serve as a channel material for electronic devices. Similar to the case of graphene, electrical properties of GO are very sensitive to the surface adsorbates,[7–9] which stimulated a number of studies that focused on rGO-based gas sensors.[10–19]

Compared to pristine graphene, rGO has many advantages as a material for gas sensing. rGO could be synthesized in large quantities from inexpensive reagents using simple chemical approaches.[20] It readily exfoliates to thin sheets in water, segregates at the water–air interface upon solvent evaporation,[21] and could be easily processed into continuous paper-like films.[22,23] Properties of rGO, such as conductivity, tensile strength, *etc.*, strongly depend on the degree of GO reduction,[24,25] which means that they could be finely tuned by the reduction conditions. Rich chemistry of rGO allows for further chemical modification with different functional groups,[2,3] which potentially makes rGO a very versatile platform for gas sensing.

Some of the studies on rGO-based gas sensors are discussed in the recent review articles.[26–28] Several papers report on rGO sensors capable of detection of chemically aggressive gases, such as NO_2, NH_3,[14,16,29] Cl_2 (ref. 16) and NO,[17] with typical response and recovery times of about several tens of minutes.[26] The demonstrated response of an rGO sensor to some chemical warfare agents and explosives at parts-per-billion (ppb) levels[10] showed the potential of these sensors for homeland security purposes. Recent studies on gas sensing by rGO also include various modifications in both sensor material (for instance, decoration of rGO with palladium nanoparticles[17]) and sensor design (*e.g.* gas detection by rGO-based field effect transistors[18]).

Despite all advantages of rGO for sensing applications, rGO-based gas sensors require many improvements to be made. Different gas molecules could be adsorbed on the surface of an rGO flake and change its conductivity, which would result in a poor selectivity of rGO-based sensors. Although a recent study suggests that some analytes could be recognized by their distinguishably different effects on the low-frequency noise spectra of graphene,[30] it remains unclear if a similar recognition

[a]*Department of Chemistry, University of Nebraska – Lincoln, Lincoln, NE, 68588, USA. E-mail: sinitskii@unl.edu*

[b]*Department of Physics, Saratov State Technical University, Saratov, 410054, Russian Federation*

[c]*Department of Physics, Southern Illinois University, Carbondale, IL, 62901, USA. E-mail: akolmakov@physics.siu.edu*

[d]*Nebraska Center for Materials and Nanoscience, University of Nebraska – Lincoln, Lincoln, NE, 68588, USA*

This journal is © The Royal Society of Chemistry 2013

Published on 12 April 2013. Downloaded by UNIVERSITY OF NEBRASKA on 16/07/2013 09:18:29.

could be performed using rGO sensors. Furthermore, such sensors are typically fabricated from rGO films in which many flakes of different size, shape, thickness, and degree of reduction partially overlap forming random junctions. The conductivity of different flakes themselves could vary by at least an order of magnitude,[31,32] and the random junctions between such flakes may cause even larger variability in electrical properties of rGO films. As a result, sensor performance of different devices prepared from such films may exhibit a significant device-to-device variation even if the same fabrication protocol was followed and rGO samples from the same batch were used.[18]

In this paper we demonstrate that significant device-to-device variability of rGO-based sensors may actually be used as an advantage to solve the problem of their poor selectivity. A large array of integrated rGO devices that have sufficiently different electronic properties could be considered as an electronic analog of an olfactory system (a so-called "electronic nose" or "e-nose").[33] The electronic nose concept was first introduced in eighties[34] to mimic the olfactory system of mammals using sensor arrays as partially selective receptors, and digital signal processing[35,36] combined with pattern recognition methods.[37–39] In such an artificial olfactory system, the analyte adsorption events become converted into an array (vector) of electrical signals. The signals from all non-specific individual sensors with partially overlapping selectivities are collected, and a pattern recognition algorithm places the vector responses into areas in a multidimensional odor space that correspond to the gases that the system is calibrated ("trained") to detect. After this training, a library of patterns of "known" odor classes is created, and newly measured "unknown" gas patterns are compared to these "known" classes. If an analyzed odor is identical to one of the gases already known by the system, its signal pattern should fall into the corresponding area in the odor space manifesting a recognition event.

Recently, multielectrode e-nose systems comprising devices based on other low dimensional oxide materials were shown to reliably detect and recognize different gas analytes.[40–46] Two recent studies also report on multiple arrays of GO/fluorophore sensing elements that were used for the optical detection of biological analytes in a solution.[47,48] In all these examples, a significant device-to-device variation is the key requirement for an electronic nose system (see reviews 49 and 50 and references therein), which, as we discussed above, is an intrinsic property of multiple rGO sensors. Thus, in this work we took advantage of the structural and electronic non-uniformity of rGO films to construct a highly selective gas sensor system. We fabricated an integrated array of weakly selective sensing elements that was employed to recognize different alcohols, such as methanol, ethanol and isopropanol. The experiments were performed in a nearly practical gaseous environment, *i.e.* under atmospheric pressure, in a dry air background and at room temperature. As chemically similar analytes, the above alcohols would be a challenge to discriminate by an e-nose sensor system. Such sensors could be of practical importance due to the dramatically different impact of selected alcohols on human health. To the best of our knowledge, this is the first demonstration of an rGO-based gas sensing device that could reliably recognize analytes of nearly the same chemical nature.

GO flakes were produced using the method recently reported by Marcano *et al.*[32] and characterized by scanning electron microscopy (SEM), X-ray photoemission spectroscopy (XPS), Raman spectroscopy and X-ray diffraction (XRD) analysis (Fig. 1). According to the SEM results, lateral dimensions of synthesized GO flakes were very different, ranging from a few hundred nm up to ~200 μm (Fig. 1a). The C1s XPS spectrum of the as-prepared GO shows that the material was heavily oxidized (Fig. 1b): the peak at 284.8 eV corresponds to the C–C bond, whereas the very intense overlapping peaks at 286–289 eV correspond to the carbon in different oxygen-containing functionalities.[9,51] Fig. 1c shows the Raman spectrum of the as-prepared GO that exhibits a D band at 1363 cm^{-1} and a G band at 1594 cm^{-1} with comparable intensities, which is typical for such heavily oxidized materials.[9,51] According to the results of XRD analysis, the average distance between GO monolayers was ~8 Å (Fig. 1d), which is in agreement with previously reported XRD data for similar heavily oxidized GO materials.[29,32,52–56]

The GO platelets were dispersed in distilled water to yield a 0.05 mg ml^{-1} solution, which was drop-cast on a modified KAMINA multisensor chip (Fig. 2a).[57] The active area of this chip consists of a 8 × 10 mm^2 Si/SiO_2 substrate with pre-deposited multiple Pt electrodes (100 × 3000 μm^2 each) separated by

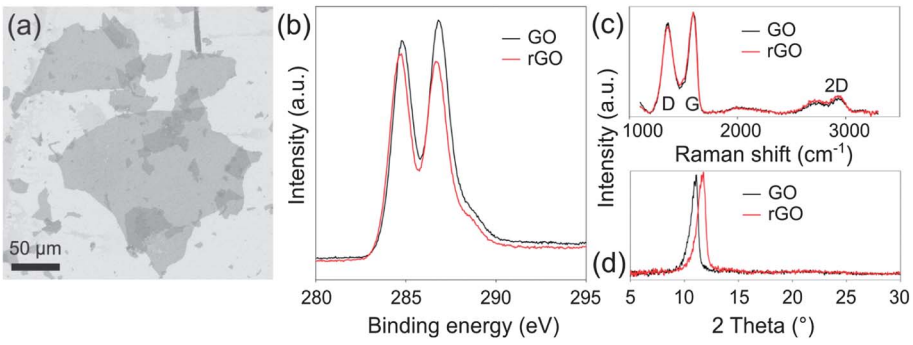

Fig. 1 Characterization of GO and rGO. (a) SEM image of the as-prepared GO flakes deposited on a Si/SiO_2 substrate. (b) XPS, (c) Raman and (d) XRD spectra of the as-prepared GO and rGO, which was annealed in vacuum at 150 °C.

Published on 12 April 2013. Downloaded by UNIVERSITY OF NEBRASKA on 16/07/2013 09:18:29.

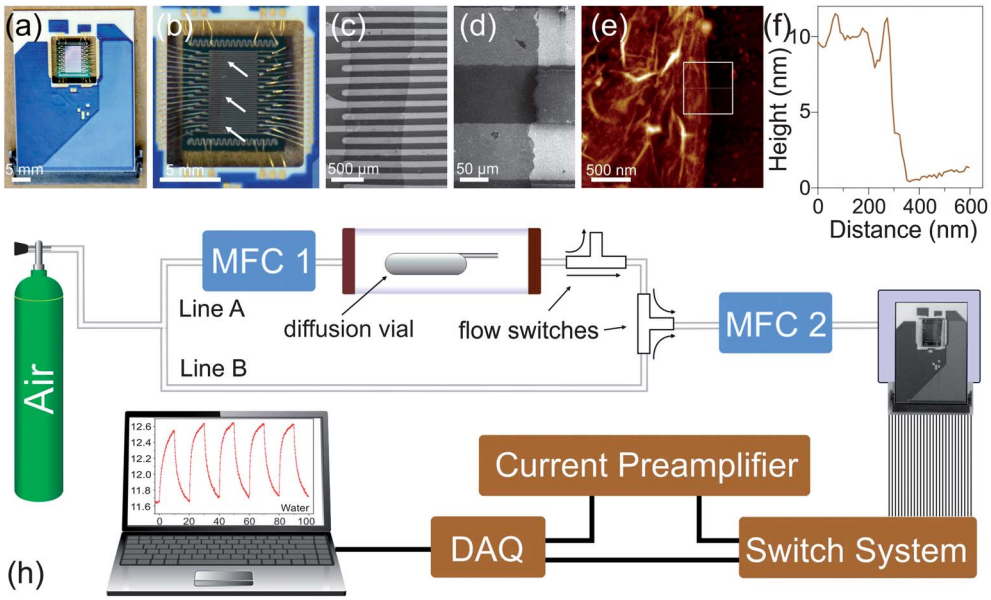

Fig. 2 rGO-based multisensor array. (a) Optical photograph of a multielectrode KAMINA chip. The following images (b)–(e) show sequential magnifications of the chip. (b) Optical photograph of the active part of the KAMINA chip. The white arrows show a dark vertical strip that corresponds to an rGO film. (c) SEM image of rGO sensors. Bright horizontal lines correspond to Pt electrodes; darker vertical strip corresponds to rGO. (d) SEM image of a fragment of one of the devices shown in (c). (e) AFM image of an rGO film on a Si/SiO_2 substrate. (f) An average height profile for the area shown by the square in (e). (h) The experimental setup for sensor measurements (see the Experimental section for details).

~90 μm gaps, and two Pt thermoresistors; the back side of the substrate is equipped with four independent Pt meander heaters. The solvent evaporation resulted in the formation of a multilayer GO film covering the Pt electrodes and the gaps between them. SEM images of this film show that the arrangement of the GO flakes varies throughout the substrate (Fig. 2c and d). According to the results of AFM, the average thickness of the GO film was 10 ± 2 nm (Fig. 2e and f). Assuming that the height of a GO monolayer is ~1 nm,[58] the film consisted of ~10 layers of GO.

The as-prepared GO is heavily oxidized and thus not electrically conductive.[4,5] In order to partially reduce GO and increase its conductivity we annealed the GO film deposited on a KAMINA chip at 150 °C in vacuum ($p = 2 \times 10^{-5}$ Torr) for 3 min. After such annealing, the resulting rGO is sufficiently conductive for further sensor measurements, although it is only partially reduced and still has numerous oxygen-containing functionalities, as shown by XPS. Fig. 1b demonstrates the C1s XPS spectrum of the rGO annealed at 150 °C in vacuum where the intensity of the overlapping peaks at 286–289 eV only slightly decreased compared to the spectrum of the as-prepared GO. The Raman spectra of GO and rGO also look very similar (Fig. 1c) suggesting that the annealing at 150 °C did not change the structure of the material significantly. The results of XPS and Raman spectroscopy are also in good agreement with the XRD data presented in Fig. 1d. An oxidized GO material typically has an average interplanar distance d ranging from 7 to 9 Å (ref. 29, 32, 53–56) depending on the exact preparation technique and XRD experimental conditions, such as humidity.[52] An extensive chemical reduction of GO results in a dramatic decrease in d to ~3.5 Å,[29,53,55,56] which is associated with the removal of the majority of functional groups from GO sheets. In contrast, Fig. 1d shows that during annealing at 150 °C the average interplanar distance in a GO material only slightly decreased from 8 to 7.6 Å, which again confirms that the structure of the GO material did not change significantly upon thermal reduction at 150 °C.

The degree of rGO reduction is known to have a profound effect on the rGO sensor performance. Conductometric rGO-based gas sensors have relatively long recovery time after exposure to an analyte under ambient conditions.[10,12] When the sensor is not fully recovered, the conductivity baseline drifts from one sensing cycle to another. This makes the sensing response irreproducible even at the same analyte concentration. The use of higher temperatures for reduction of GO results in the enhancement of the response but also leads to much longer recovery times.[14] Therefore, to address the problem of run-to-run changes in the conductance baseline we chose the reduction conditions at which the GO was only slightly reduced (Fig. 1b and c) but yet sufficiently conductive to perform electrical measurements.

Fig. 2b shows that the conductive rGO film bridges 39 sequential electrodes thus forming 38 devices with Pt electrodes and active rGO channels. Fig. 2h shows the experimental setup that was used to measure the rGO resistance between each pair of electrodes in the array, see the Experimental section for more details. We evaluated the ability of an rGO microarray to discriminate between different alcohols: methanol, isopropanol and ethanol. The I–V and I–t characteristics have been studied in a 20 sccm flow of synthetic air (21% of O_2, 79% of N_2) mixed with alcohol vapors at three different concentrations: 500, 1000 and 1500 ppm. The time of exposure of rGO sensors to the

 This journal is © The Royal Society of Chemistry 2013

Published on 12 April 2013. Downloaded by UNIVERSITY OF NEBRASKA on 16/07/2013 09:18:29.

analyte gases was chosen to be 10 min, which was found in preliminary measurements to be long enough to ensure the saturation of the sensor signal.

The rGO has an irregular atomic structure that comprises nearly perfect graphene domains, oxidized regions and nanoscopic holes.[59] Once it is exposed to air, gas molecules adsorb at different sites in this complex material changing its conductivity, as shown in Fig. 3a. After annealing in vacuum at 150 °C the rGO devices had resistances ranging from 0.2 to 0.7 MOhm. Fig. 3a shows that when these devices were tested within 1 h after the exposure to air, their resistances increased by about an order of magnitude. The following measurements demonstrate the resistances of rGO devices almost saturated after ~1 day of exposure to air in the 5–15 MOhm range (Fig. 3a). Therefore, to eliminate the effect of adsorbates that are present in air on the sensor properties of rGO we kept the devices in air at room temperature for several days before the sensor measurements. Fig. 3b demonstrates that the rGO devices exhibited linear *I–V* curves, which implies an Ohmic contact between rGO sheets and Pt electrodes; a line corresponding to the as-prepared non-conducting GO is shown for comparison.

Fig. 3c shows a typical sensor response of an individual rGO gas sensor to isopropanol, methanol, ethanol and water that were mixed with dry synthetic air at a 1500 ppm concentration. When an rGO device is exposed to any of these four analytes its resistance increases, but it could be recovered if the device is then purged with dry air. Fig. 3c demonstrates five exposure–purge cycles for each of these analytes, showing that the corresponding resistance changes are quite reproducible. The response curves clearly consist of regions with sharp and

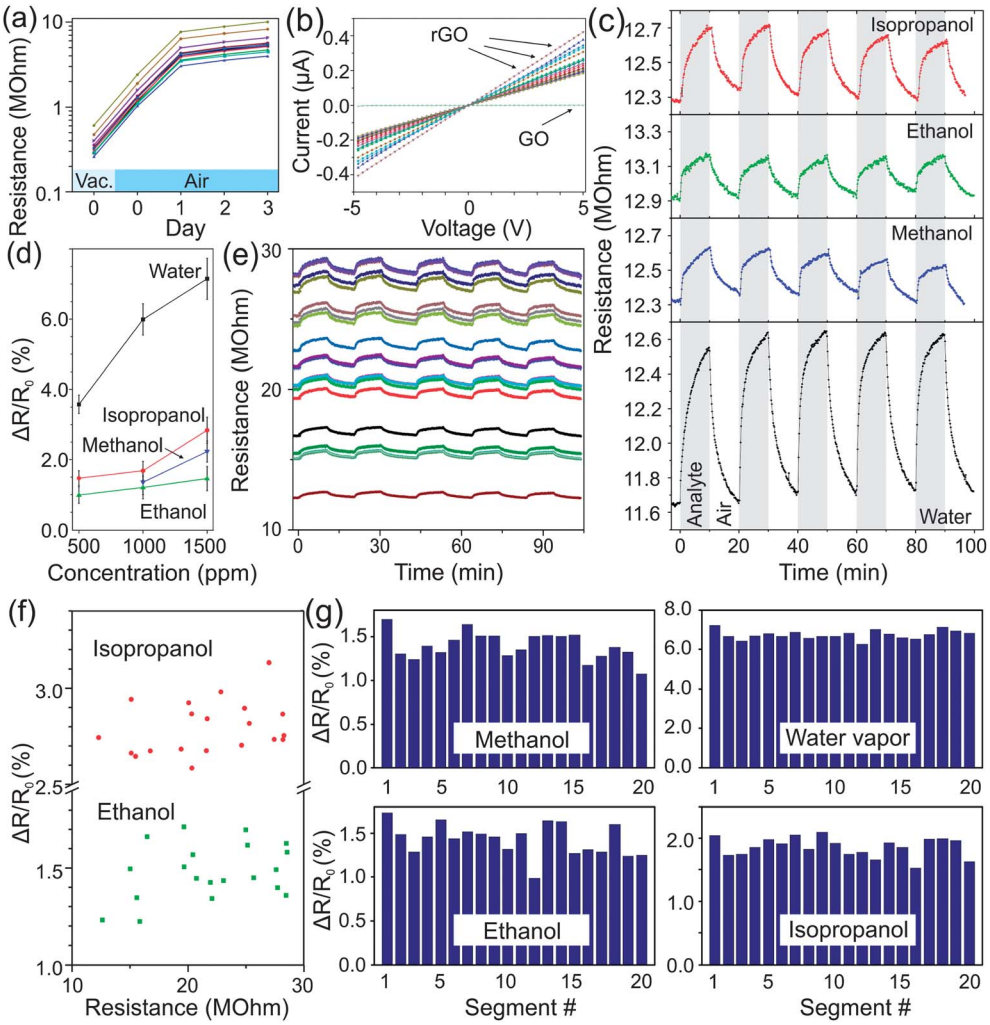

Fig. 3 Sensor characteristics of an rGO-based multisenor array. (a) Resistances of 13 rGO-based devices measured in vacuum and in air. (b) Current–voltage (*I–V*) curves for 13 rGO-based devices; an almost horizontal line shows a representative *I–V* curve for an as-made GO device for comparison. (c) Representative dynamic behavior of one of the rGO-based devices in a multisensor array, which was exposed to 1500 ppm of an analyte in synthetic air. Gray and white vertical lines correspond to periods of time when the flow of an analyte was turned on and off, respectively. (d) Dependence of relative resistance changes ($\Delta R/R_0$) of rGO devices on concentrations of different analytes. Each data point is an average of 80 independent measurements (4 times × 20 rGO devices). The error bars show maximum and minimum values for each dataset. (e) Simultaneously measured dynamic behaviors of 20 rGO devices that experienced 5 cycles of exposure to 1000 ppm of isopropanol followed by purging with dry air. (f) Dependence of relative resistance changes ($\Delta R/R_0$) on initial resistances of rGO devices upon exposure to 1500 ppm of isopropanol or ethanol in synthetic air. (g) Distributions of gas responses of rGO segments to different analytes.

Published on 12 April 2013. Downloaded by UNIVERSITY OF NEBRASKA on 16/07/2013 09:18:29.

moderate slopes that correspond to fast and slow responses of an rGO sensor to the analytes, respectively; such behavior is apparent in cases of methanol and ethanol exposure, and also develops in the isopropanol and to a lesser extent water response curves after the initial cycle, see Fig. 3c. According to Robinson *et al.*, the fast response could be attributed to the adsorption of molecules at the low-energy binding sites, such as sp^2 carbon domains, while the slow response was mainly caused by interactions between gas molecules with high-energy binding sites, such as vacancies, defects, and oxygen-containing functionalities.[10,18] Once an rGO sensor is exposed to a new analyte, the analyte molecules may be retained at some of these high-energy binding sites after the first cycle, eliminating the contribution of these sites to the sensor response in the following cycles. This could explain the fact that in many series of measurements the first cycle was often substantially different from the following ones (an example of this effect could be seen in the water sensing data shown in Fig. 3c).

Fig. 3d shows average responses of 20 rGO segments to ethanol, methanol, isopropanol and water vapor at different concentrations. Each segment was measured 5 times, and the first data points in each series were not considered for this plot for the reason discussed above. The data are shown in terms of $\Delta R/R_0$, where R_0 corresponds to the original resistance of an rGO device in a multisensor array before the exposure to an analyte and ΔR is the maximum change in the device resistance during the sensing experiment. The response of rGO devices to the water vapors is about four times higher than that of alcohols at the same concentration. This can be explained by the unusually facile permeation of water molecules between GO flakes.[52,60] Therefore, the humidity level in the air could dramatically affect the results of alcohol detection and recognition experiments. To address this problem all alcohol sensing experiments were performed after the rGO devices were purged with dry air for >1 h. If an array of rGO devices is employed as a primary sensing element in a practical electronic nose for the alcohol recognition, the water molecules should be removed by the sample collecting system,[61] possibly through the use of concentrators and dryers.

To provide a sufficient recognition power, the gas analytical array requires diversity in the sensing performance of the individual sensing segments. Fig. 3e shows simultaneous response of 20 different segments of the sensing array when exposed to 1000 ppm concentration of methanol. The observed differences in the signal amplitude and response time can be used for discrimination between alcohol analytes when all these 20 segments are employed for the vector signal collection. Fig. 3f shows that relative resistance changes ($\Delta R/R_0$) of rGO devices observed during their exposure to different analytes did not correlate with initial resistances (R_0) of the devices, further demonstrating their stochastic nature; the data are shown for isopropanol or ethanol exposure, similar results were obtained for other analytes as well.

Although the exact nature of the selectivity of the individual rGO sensing segments is a subject of an ongoing study, we presume that the required diversity is mainly provided by the irregular structure of rGO films at different levels of organization, ranging from nanoscale (disordered structure of individual rGO flakes[59]) to macroscale (randomly percolating junctions of rGO flakes, wrinkles, variable thickness of an rGO film). Side-by-side comparison of the responses of 20 individual rGO devices to selected analytes mixed at a 1000 ppm concentration with dry air shows the expected device-to-device variation. Fig. 3g shows that for any given analyte all 20 segments exhibit different relative changes in their electrical resistances; all these sensor responses combined give a characteristic pattern for that analyte. Characteristic patterns for ethanol, methanol, isopropanol and water look different (Fig. 3g), which could be used for the recognition of these gases. The diversity of the rGO devices could be further increased if some of them are covalently functionalized using diazonium chemistry,[62,63] which might be a promising direction for future studies.

Comparison of the patterns for different analytes shown in Fig. 3g yields an important observation regarding the nature of selectivity of rGO device arrays in the discussed gas recognition experiments. The AFM results show that the rGO film that was used in this work was ~10 layer thick. According to Nair *et al.*, water molecules could easily penetrate between the layers of GO that have a very large average interplanar distance.[60] The XRD results show that the rGO film prepared by the thermal annealing of GO at 150 °C had a d value of 7.6 Å that is very close to $d = 8$ Å found for the as-prepared GO material (Fig. 1d), suggesting that the permeation of the water molecules between the rGO layers should be substantial. As the water molecules penetrate between the rGO layers, they affect conductivities of the majority of flakes and their junctions more or less evenly, see Fig. 4. As a result, all 20 rGO devices in the array exhibit

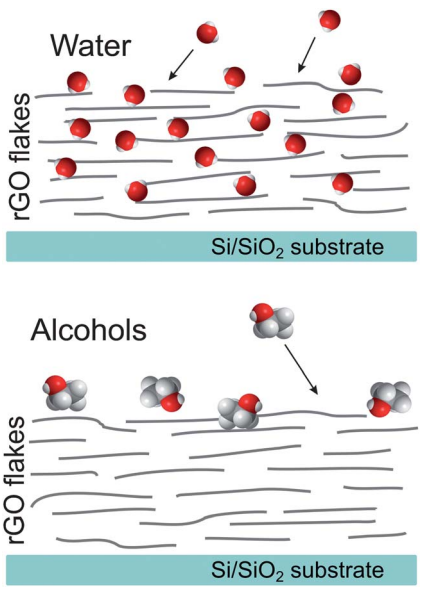

Fig. 4 Scheme of a proposed mechanism of analyte discrimination by gas sensors based on rGO films. Water molecules easily penetrate between rGO flakes, changing the bulk conductivity of a film. In contrast, molecules of alcohols result in smaller conductivity changes, since they interact only with the top few layers of an rGO film. The depth of penetration of alcohol molecules should depend on the local microstructure of a film and the chemical nature of an analyte.

This journal is © The Royal Society of Chemistry 2013

Published on 12 April 2013. Downloaded by UNIVERSITY OF NEBRASKA on 16/07/2013 09:18:29.

nearly the same relative resistance change when exposed to the water vapor, and the characteristic pattern for water is flat and nearly uniform (Fig. 3g). The latter corroborates with the large overall sensor signal toward water molecules since most of the rGO flakes in the sensing segments contribute to the conductance change. In contrast, the values of the sensing responses become smaller and the characteristic patterns appear to be more scattered for all three alcohols used in this study. It was previously experimentally demonstrated that thick GO membranes are impermeable for many gas molecules other than water, including alcohols,[60] which means that in our sensor experiments only the top few layers of the rGO film should be affected by the alcohol molecules (Fig. 4). In this case, the actual depth of penetration of analyte molecules should depend on the local near-surface microstructure of an rGO film, *i.e.* the size and geometry of rGO flakes, wrinkles, various defects, *etc.*, and thus could vary substantially for different devices in the array, resulting in their different responses to the alcohol analytes (Fig. 3g). Furthermore, for each device with its unique rGO film microstructure the effective penetration depth should also depend on the nature of an analyte, which would result in different characteristic patterns observed for ethanol, methanol, isopropanol, and obviously water (Fig. 3g). While this explanation for the selectivity mechanism seems plausible and consistent with our data as well as other studies of GO/rGO, detailed sensor experiments using rGO films with variable thickness, average flake size, degree of reduction and preparation method are necessary for its verification. Also, since a KAMINA chip has built-in resistive heaters,[57] it is an excellent platform for the sensing experiments at different temperatures, which may provide further insights into the sensing mechanism, since the kinetics of adsorption/desorption of analyte molecules should be temperature-dependent.

A perception-type artificial neural network (ANN)[64] has been employed to analyze the signal responses of the developed multisensor chip. Linear regions corresponding to the "slow response" phases from 20 rGO devices (P_i, $i = 1$ to 20) were used as the input data and then transformed to only two output signals X and Y (Fig. 5a) by means of activation functions (f_i) and weight factors (W_i). After every training cycle, the Levenberg–Marquardt algorithm[65] modified weight factors to minimize the mean squared error (a so-called "training goal") of the distances between the resulting output XY-vectors and the manually assigned gravity center for a certain analyte. The gravity centers assigned in this analysis are (0.5, 1) – water, (1, 0.5) – ethanol, (0.5, 0) – isopropanol, and (0, 0.5) – methanol. The training data consisted of 25 recognition experiments for each analyte. The training goals equal to 10^{-3} and 10^{-9} were reached in 12 and 42 training cycles respectively, showing that more accurate recognition requires longer data processing.

ANN performance was tested using 25 sets of multisensor array resistance records corresponding to each of the gas analytes which were not employed in the training process. As shown in Fig. 5b, the ANN trained at the goal equal to 10^{-3} could

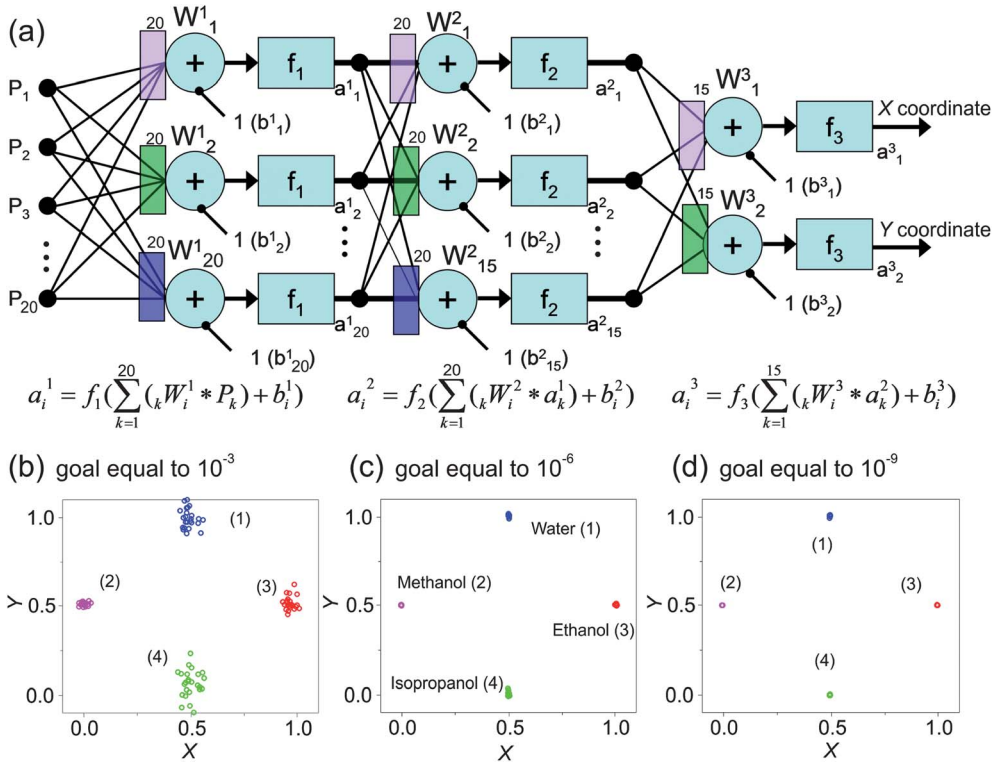

Fig. 5 Analyte recognition by an rGO-based multisensor array. (a) The scheme of the ANN employed in the study that transforms the input sensor data (P_i, $i = 1$ to 20) from 20 rGO segments in the multisensory array to two output signals, X and Y; see text for details. (b–d) The results of recognition of water (1), methanol (2), ethanol (3) and isopropanol (4) by the ANN at training goals equal to (b) 10^{-3}, (c) 10^{-6}, and (d) 10^{-9}; see text for details.

Published on 12 April 2013. Downloaded by UNIVERSITY OF NEBRASKA on 16/07/2013 09:18:29.

completely recognize all four analytes, unambiguously attributing every tested gas to one of four gravity centers. Longer trainings of the ANN at the goals equal to 10^{-6} and 10^{-9} (Fig. 5c and d) clearly improve the gas discrimination.

In summary, we have demonstrated that rGO-sensor arrays could be used to effectively distinguish between chemically akin analytes, such as methanol, ethanol and isopropanol. Advantages of such sensors for potential practical applications include facile and inexpensive synthesis of GO, its convenient deposition on commercially available multielectrode chips followed by a simple low-temperature thermal conversion to rGO, and the good recognition performance. Future work will focus on the better understanding of the sensing mechanism, optimization of the sensor performance, and recognition of other practically important analytes.

Experimental

Synthesis of GO

All reagents were purchased from Aldrich and used as received. Graphite flakes (1.7 g), $KMnO_4$ (8 g), H_2SO_4 (180 ml) and H_3PO_4 melted at 45 °C (30 g) were mixed in that order in an ice bath. The dispersion was stirred at room temperature for 3 days, quenched with H_2O_2 in an ice bath, and then centrifuged at 7000 rpm for 30 min. The resulting solvent phase was clear and the solid phase had a yellow-brown color. The solid was dispersed in water and centrifuged again. The procedure was repeated several times until pH = 4. The resulting GO solution had a concentration of 2.5 mg ml^{-1}.

Materials characterization

SEM was performed using a Hitachi S4700 field-emission scanning electron microscope at an accelerating voltage of 5 kV. The Raman spectra were collected using a Thermo Scientific DXR Raman microscope with a 532 nm excitation laser. XPS was performed using a PHI Quantera SXM scanning X-ray microprobe. AFM images were recorded using a Digital Instruments Nanoscope IIIa Dimension 3100 system and Bruker RTESPA AFM probes (part # MPP-11120-10). XRD patterns were collected using a Rigaku automated Powder X-ray diffractometer with a Theta–Theta goniometer (monochromatic CuKα_1 radiation with $\lambda = 1.54056$ Å; $5^\circ \leq 2\theta \leq 30^\circ$).

Gas sensing measurements

The setup for gas sensing measurements is shown in Fig. 2h. Two-terminal resistance measurements of individual sensing elements in the array were performed at a constant voltage mode using a low noise current preamplifier (Stanford Research Systems, model SR570). The latter was connected to a Keithley 7001 Switch System that was sequentially reading the current from every individual sensing element in the array. The entire setup was connected to a computer through a National Instruments data acquisition board (DAQ) *via* a BNC-2110 connector block and controlled using a National Instruments LabView software. The chip was placed into a gas exposure chamber ($V \sim 2$ cm^3) kept at the ambient temperature. An analyte was put in a vial with a custom-made horizontal capillary diffusion tube (Fig. 2h). If this diffusion vial is kept at a constant temperature, the concentration gradient of the analyte inside and outside the vial remains constant, which provides the constant driving force for a controlled release of the analyte to the flow of synthetic air. The bore diameter and diffusion path length determine the release rate for a specific analyte. Eqn (1) was used to calculate the diffusion path length:

$$L = 1.9 \times 10^4 TDMA \frac{\log P}{P - \rho} K \frac{1}{FC}, \quad (1)$$

where L is the length of the diffusion path (cm), T is the temperature of the vapor (K), D is the diffusion coefficient (cm^2 s^{-1}) at 25 °C and 1 atm, M is the molecular weight (g mol^{-1}), A is the cross-section area of the capillary (cm^2), P is the atmospheric pressure (mm Hg), ρ is the vapor pressure at the temperature T (mm Hg), K is the molar volume constant at 25 °C and at 1 atm ($K = 24.47/M$), F is the total dilution flow (sccm), and C is the concentration (parts per million (ppm) by volume).

We used Line A to expose the rGO devices to an analyte and Line B to purge them with a dry air (Fig. 2h). Two independent mass flow controllers (MFC, Matheson Transducer, Model 8141) were used to maintain the same gas flow rates through both lines, and two flow switches were used to open or close these lines. When the rGO devices where purged with dry air through Line B, the chamber with the diffusion vial was also continuously purged with dry air to prevent the accumulation of an analyte in the chamber.

Recognition data processing

To be able to distinguish vector signals related to different classes the ANN was preliminary trained. During every training session, input data of the sensor resistances (vector P) were multiplied by the weight factors W^1 of neurons of the first layer. The obtained products were summarized and processed by means of the activation function f_1. The output vector of the first layer was used in the next layer and processed in a similar manner with weight factors W^2 and activation function f_2. The activation functions, f_1 and f_2, were assigned to be logarithmic-sigmoid, which can be differentiated and allow one to use the training algorithms based on the gradient descent. The activation function f_3 of the output layer, in contrast, was linear.

After processing in the intermediate layers, the data were sent to the output layer that was composed of two neurons. To visualize the output recognition of gases we assigned a 2-dimensional plane where *X*- and *Y*-axes corresponded to output neurons 1 and 2 respectively. Thus, the ANN projects the primary 20-dimensional signal from the individual segments of the multisensor array to the 2D *XY*-plane. The gravity centers for the output data corresponding to different analytes were assigned as follows: (0.5, 1) – water, (1, 0.5) – ethanol, (0.5, 0) – isopropanol, and (0, 0.5) – methanol.

The Levenberg–Marquardt algorithm[65] was used to train the ANN which modifies the neuron weights to achieve the minimum value of the training goal. One cycle of the modification of the weight factors in the ANN stands for one training

 This journal is © The Royal Society of Chemistry 2013

Published on 12 April 2013. Downloaded by UNIVERSITY OF NEBRASKA on 16/07/2013 09:18:29.

cycle. The training data consisted of 25 resistance records for each analyte (ethanol, methanol, isopropanol and water vapor). Each record is a 20-dimensional vector obtained from individual segments of the rGO sensor array. The ANN training results in the projections of the sensor responses of 20 rGO segments to the 2D *XY*-plane. The ANN was found to recognize the analytes after only a few training cycles. The goal equal to 10^{-3} was achieved after 12 training cycles, and the goal equal to 10^{-9} was achieved after 42 training cycles.

ANN performance was tested using 25 sets of multisensor resistance records under exposure to each of the gas analytes which were not employed in the training process.

Acknowledgements

The work at UNL was funded by the Nebraska Public Power District through the Nebraska Center for Energy Sciences Research (#12-00-13) and the NSF through Nebraska MRSEC (DMR-0820521) and EPSCoR (EPS-1004094). The research at SIUC was supported through the NSF ECCS-0925837 grant. V.S. and A.V. thank the partial support from the Russian Ministry of Education and Science, grant #14.B37.21.1076. The authors thank Mikhail Shekhirev for the AFM characterization of GO films.

References

1 F. Schedin, A. K. Geim, S. V. Morozov, E. W. Hill, P. Blake, M. I. Katsnelson and K. S. Novoselov, *Nat. Mater.*, 2007, **6**, 652–655.
2 D. R. Dreyer, S. Park, C. W. Bielawski and R. S. Ruoff, *Chem. Soc. Rev.*, 2010, **39**, 228–240.
3 A. Sinitskii and J. M. Tour, in *Graphene Nanoelectronics: From Materials to Circuits*, ed. R. Murali, Springer, New York, NY, 2012, ch. 8, pp. 205–234.
4 C. Gómez-Navarro, R. T. Weitz, A. M. Bittner, M. Scolari, A. Mews, M. Burghard and K. Kern, *Nano Lett.*, 2007, **7**, 3499–3503.
5 S. Gilje, S. Han, M. Wang, K. L. Wang and R. B. Kaner, *Nano Lett.*, 2007, **7**, 3394–3398.
6 A. Sinitskii, A. A. Fursina, D. V. Kosynkin, A. L. Higginbotham, D. Natelson and J. M. Tour, *Appl. Phys. Lett.*, 2009, **95**, 253108.
7 G. Eda, G. Fanchini and M. Chhowalla, *Nat. Nanotechnol.*, 2008, **3**, 270–274.
8 I. Jung, D. A. Dikin, R. D. Piner and R. S. Ruoff, *Nano Lett.*, 2008, **8**, 4283–4287.
9 A. Sinitskii, A. Dimiev, D. V. Kosynkin and J. M. Tour, *ACS Nano*, 2010, **4**, 5405–5413.
10 J. T. Robinson, F. K. Perkins, E. S. Snow, Z. Wei and P. E. Sheehan, *Nano Lett.*, 2008, **8**, 3137–3140.
11 R. Arsat, M. Breedon, M. Shafiei, P. G. Spizziri, S. Gilje, R. B. Kaner, K. Kalantar-zadeh and W. Wlodarski, *Chem. Phys. Lett.*, 2009, **467**, 344–347.
12 J. D. Fowler, M. J. Allen, V. C. Tung, Y. Yang, R. B. Kaner and B. H. Weiller, *ACS Nano*, 2009, **3**, 301–306.
13 G. Lu, L. E. Ocola and J. Chen, *Appl. Phys. Lett.*, 2009, **94**, 083111.
14 G. Lu, L. E. Ocola and J. Chen, *Nanotechnology*, 2009, **20**, 445502.
15 M. Zhou, Y. Zhai and S. Dong, *Anal. Chem.*, 2009, **81**, 5603–5613.
16 V. Dua, S. P. Surwade, S. Ammu, S. R. Agnihotra, S. Jain, K. E. Roberts, S. Park, R. S. Ruoff and S. K. Manohar, *Angew. Chem., Int. Ed.*, 2010, **49**, 2154–2157.
17 W. Li, X. Geng, Y. Guo, J. Rong, Y. Gong, L. Wu, X. Zhang, P. Li, J. Xu, G. Cheng, M. Sun and L. Liu, *ACS Nano*, 2011, **5**, 6955–6961.
18 G. Lu, S. Park, K. Yu, R. S. Ruoff, L. E. Ocola, D. Rosenmann and J. Chen, *ACS Nano*, 2011, **5**, 1154–1164.
19 J. Wang, Y. Kwak, I.-y. Lee, S. Maeng and G.-H. Kim, *Carbon*, 2012, **50**, 4061–4067.
20 M. Segal, *Nat. Nanotechnol.*, 2009, **4**, 612–614.
21 M. Krueger, S. Berg, D. Stone, E. Strelcov, D. A. Dikin, J. Kim, L. J. Cote, J. X. Huang and A. Kolmakov, *ACS Nano*, 2011, **5**, 10047–10054.
22 N. I. Kovtyukhova, P. J. Ollivier, B. R. Martin, T. E. Mallouk, S. A. Chizhik, E. V. Buzaneva and A. D. Gorchinskiy, *Chem. Mater.*, 1999, **11**, 771–778.
23 D. A. Dikin, S. Stankovich, E. J. Zimney, R. D. Piner, G. H. B. Dommett, G. Evmenenko, S. T. Nguyen and R. S. Ruoff, *Nature*, 2007, **448**, 457–460.
24 I. Jung, D. A. Field, N. J. Clark, Y. W. Zhu, D. X. Yang, R. D. Piner, S. Stankovich, D. A. Dikin, H. Geisler, C. A. Ventrice and R. S. Ruoff, *J. Phys. Chem. C*, 2009, **113**, 18480–18486.
25 A. Mathkar, D. Tozier, P. Cox, P. J. Ong, C. Galande, K. Balakrishnan, A. L. M. Reddy and P. M. Ajayan, *J. Phys. Chem. Lett.*, 2012, **3**, 986–991.
26 S. Basu and P. Bhattacharyya, *Sens. Actuators, B*, 2012, **173**, 1–21.
27 F. Yavari and N. Koratkar, *J. Phys. Chem. Lett.*, 2012, **3**, 1746–1753.
28 Q. He, S. Wu, Z. Yin and H. Zhang, *Chem. Sci.*, 2012, **3**, 1764–1772.
29 L. J. Cote, R. Cruz-Silva and J. X. Huang, *J. Am. Chem. Soc.*, 2009, **131**, 11027–11032.
30 S. Rumyantsev, G. X. Liu, M. S. Shur, R. A. Potyrailo and A. A. Balandin, *Nano Lett.*, 2012, **12**, 2294–2298.
31 C. Gomez-Navarro, R. T. Weitz, A. M. Bittner, M. Scolari, A. Mews, M. Burghard and K. Kern, *Nano Lett.*, 2007, **7**, 3499–3503.
32 D. C. Marcano, D. V. Kosynkin, J. M. Berlin, A. Sinitskii, Z. Z. Sun, A. Slesarev, L. B. Alemany, W. Lu and J. M. Tour, *ACS Nano*, 2010, **4**, 4806–4814.
33 T. C. Pearce, S. S. Schiffman, H. T. Nagle and J. W. Gardner, *Handbook of Machine Olfaction: Electronic Nose Technology*, Wiley-VCH Verlag GmbH & Co. KGaA, Weinheim, 2003.
34 K. Persaud and G. Dodd, *Nature*, 1982, **299**, 352–355.
35 T. C. Pearce, *BioSystems*, 1997, **41**, 43–67.
36 J. A. Riffell, H. Lei, L. Abrell and J. G. Hildebrand, *Science*, 2013, **339**, 200–204.

Published on 12 April 2013. Downloaded by UNIVERSITY OF NEBRASKA on 16/07/2013 09:18:29.

37 E. L. Hines, J. W. Gardner and C. E. R. Potter, *Meas. Control*, 1997, **30**, 262–268.
38 C. Di Natale, A. Macagnano, A. D'Amico and F. Davide, *Meas. Sci. Technol.*, 1997, **8**, 1236–1243.
39 S. Ampuero and J. O. Bosset, *Sens. Actuators, B*, 2003, **94**, 1–12.
40 P. C. Chen, G. Z. Shen and C. W. Zhou, *IEEE Transactions on Nanotechnology*, 2008, **7**, 668–682.
41 V. V. Sysoev, E. Strelcov, M. Sommer, M. Bruns, I. Kiselev, W. Habicht, S. Kar, L. Gregoratti, M. Kiskinova and A. Kolmakov, *ACS Nano*, 2010, **4**, 4487–4494.
42 J. M. Baik, M. Zielke, M. H. Kim, K. L. Turner, A. M. Wodtke and M. Moskovits, *ACS Nano*, 2010, **4**, 3117–3122.
43 V. V. Sysoev, E. Strelcov, S. Kar and A. Kolmakov, *Thin Solid Films*, 2011, **520**, 898–903.
44 E. N. Dattoli, A. V. Davydov and K. D. Benkstein, *Nanoscale*, 2012, **4**, 1760–1769.
45 C. J. Belle and U. Simon, *J. Mater. Res.*, 2013, **28**, 574–588.
46 S. Hwang, H. Kwon, S. Chhajed, J. W. Byon, J. M. Baik, J. Im, S. H. Oh, H. W. Jang, S. J. Yoon and J. K. Kim, *Analyst*, 2013, **138**, 443–450.
47 H. Pei, J. Li, M. Lv, J. Y. Wang, J. M. Gao, J. X. Lu, Y. P. Li, Q. Huang, J. Hu and C. H. Fan, *J. Am. Chem. Soc.*, 2012, **134**, 13843–13849.
48 S. S. Chou, M. De, J. Y. Luo, V. M. Rotello, J. X. Huang and V. P. Dravid, *J. Am. Chem. Soc.*, 2012, **134**, 16725–16733.
49 A. Hierlemann and R. Gutierrez-Osuna, *Chem. Rev.*, 2008, **108**, 563–613.
50 F. Rock, N. Barsan and U. Weimar, *Chem. Rev.*, 2008, **108**, 705–725.
51 S. Stankovich, D. A. Dikin, R. D. Piner, K. A. Kohlhaas, A. Kleinhammes, Y. Jia, Y. Wu, S. T. Nguyen and R. S. Ruoff, *Carbon*, 2007, **45**, 1558–1565.
52 A. Buchsteiner, A. Lerf and J. Pieper, *J. Phys. Chem. B*, 2006, **110**, 22328–22338.
53 A. B. Bourlinos, D. Gournis, D. Petridis, T. Szabo, A. Szeri and I. Dekany, *Langmuir*, 2003, **19**, 6050–6055.
54 D. V. Kosynkin, A. L. Higginbotham, A. Sinitskii, J. R. Lomeda, A. Dimiev, B. K. Price and J. M. Tour, *Nature*, 2009, **458**, 872–876.
55 D. R. Dreyer, S. Murali, Y. W. Zhu, R. S. Ruoff and C. W. Bielawski, *J. Mater. Chem.*, 2011, **21**, 3443–3447.
56 S. F. Pei, J. P. Zhao, J. H. Du, W. C. Ren and H. M. Cheng, *Carbon*, 2010, **48**, 4466–4474.
57 P. Althainz, A. Dahlke, M. Frietsch-Klarhof, J. Goschnick and H. J. Ache, *Sens. Actuators, B*, 1995, **25**, 366–369.
58 A. Sinitskii, D. V. Kosynkin, A. Dimiev and J. M. Tour, *ACS Nano*, 2010, **4**, 3095–3102.
59 K. Erickson, R. Erni, Z. Lee, N. Alem, W. Gannett and A. Zettl, *Adv. Mater.*, 2010, **22**, 4467–4472.
60 R. R. Nair, H. A. Wu, P. N. Jayaram, I. V. Grigorieva and A. K. Geim, *Science*, 2012, **335**, 442–444.
61 T. M. Dymerski, T. M. Chmiel and W. Wardencki, *Rev. Sci. Instrum.*, 2011, **82**, 111101.
62 J. R. Lomeda, C. D. Doyle, D. V. Kosynkin, W. F. Hwang and J. M. Tour, *J. Am. Chem. Soc.*, 2008, **130**, 16201–16206.
63 A. Sinitskii, A. Dimiev, D. A. Corley, A. A. Fursina, D. V. Kosynkin and J. M. Tour, *ACS Nano*, 2010, **4**, 1949–1954.
64 T. Khanna, *Foundations of neural networks*, Addison-Wesley, Redwood City, CA, 1990.
65 K. Levenberg, *Q. Appl. Math.*, 1944, **2**, 164–168.

 This journal is © The Royal Society of Chemistry 2013